arXiv:1010.5070v3 [cond-mat.str-el] 28 Mar 2011

High-field electron spin resonance spectroscopy study of $GdO_{1-x}F_xFeAs$ superconductors

A. Alfonsov[1], F. Murányi[2], V. Kataev[1], G. Lang[1], N. Leps[1], L. Wang[1], R. Klingeler[3], A. Kondrat[1], C. Hess[1], S. Wurmehl[1], A. Köhler[1], G. Behr[1], S. Hampel[1], M. Deutschmann[1], S. Katrych[4], N. D. Zhigadlo[4], Z. Bukowski[4], J. Karpinski[4], and B. Büchner[1]

[1] *IFW Dresden, Institute for Solid State Research, 01069 Dresden, Germany*
[2] *Universität Zürich - Physik-Institut, CH-8057 Zürich, Switzerland*
[3] *Kirchhoff Institute for Physics, Heidelberg University, D-69120 Heidelberg, Germany*
[4] *Laboratory for Solid State Physics, ETH Zurich, CH-8093 Zurich, Switzerland*

We report a detailed investigation of $GdO_{1-x}F_xFeAs$ ($x = 0$, 0.07 and 0.14) samples by means of high-field/high-frequency electron spin resonance (HF-ESR) together with measurements of thermodynamic and transport properties. The parent GdOFeAs compound exhibits Fe long-range magnetic order below 128 K, whereas both doped samples do not show such order and are superconducting with $T_c = 20$ K ($x = 0.07$) and $T_c = 45$ K ($x = 0.14$). The Gd^{3+} HF-ESR reveals an appreciable exchange coupling between Gd and Fe moments, through which the static magnetic order is clearly seen in the parent compound. Owing to this coupling, HF-ESR can probe sensitively the evolution of the magnetism in the FeAs planes upon F doping. It is found that in both superconducting samples, where the Fe long-range order is absent, there are short-range, static on the ESR time scale magnetic correlations between Fe spins. Their occurrence on a large doping scale may be indicative of the ground states' coexistence.

I. INTRODUCTION

Iron-pnictide superconductors[1] with superconducting critical temperatures up to 55 K[2–4] have attracted a huge interest due to striking similarities to superconducting cuprates as well as due to their original properties. Indeed, most families of these layered materials feature an antiferromagnetically (AFM) ordered parent compound, and the evolution of superconductivity concomitantly with suppression of AFM order upon doping. However there are important differences which render the Fe-pnictides a separate new class of superconducting materials. Most striking of them are semi-metallicity and the spin density wave (SDW) character of the AFM order in the undoped pnictides contrasted with the Mott-insulating AFM state in the cuprates, as well as a multi-band versus single-band electronic structure in the Fe-pnictide and cuprate high-temperature superconductors, respectively.

Beyond study of the superconducting ground state, and of the magnetic and associated structural transitions seen in the parent compound, much attention has been devoted to the issue of the ground states' coexistence. Discrepancies on this issue have been found between different families[3,5–11], with the variation of the boundary of the two ground states and different length scales of coexistence, especially in the so-called 1111 family. In this family, which has the composition ROFePn (R - rare earth, Pn - pnictide), the superconductivity evolves with the substitution of fluorine for oxygen. Here, replacement of one rare earth element with another can cause a significant variation of properties. Whereas in La-based *superconducting* samples there is evidence against static magnetic order in the FeAs planes[6], in the case of superconducting samples based on different magnetic rare earths (R = Sm, Nd, Ce) evidence of remanent static magnetism is found[3,11]. The situation appears complicated due to the fact that the magnetism then tends to be of a short-range order or disordered, possibly even dynamic[12], which calls for the use of local probe techniques. These two different pictures complicate the establishment of the unified phase diagram for 1111 pnictides, necessary for the full understanding of these materials. In addition, as was shown by NMR[13,14] and μSR[15] studies, there is a magnetic coupling between $4f$ (Ce, Pr and Sm) and $3d$ (Fe) moments. Such coupling of the rare earth to the FeAs plane might give an additional contribution to the difference in physical properties of different 1111-type superconductors.

In the present work we investigate the evolution of the magnetism upon fluorine doping in Gd-based 1111 compound by means of high field/high frequency electron spin resonance (HF-ESR) complemented with measurements of thermodynamic and transport properties. The ESR data reveal a significant exchange coupling of Gd- and Fe-moments in the parent GdOFeAs sample which enables the Gd^{3+} HF-ESR to probe sensitively the formation of the static SDW magnetic order in the FeAs planes. Interestingly, it is found that the signatures of such an order are still observed in the ESR spectra after doping. In particular, though long-range SDW order present at very low doping is suppressed at doping levels where superconductivity appears, our results imply static on the ESR time scale, likely short-range, magnetic correlations between Fe spins. This result suggests that $GdO_{1-x}F_xFeAs$ compounds may feature coexistence of quasi-static magnetism and superconductivity on a large doping range.

II. EXPERIMENTAL

A. Setups

The magnetization has been studied by means of a commercial SQUID magnetometer (MPMS-XL5, Quantum Design). For the thermal expansion measurements a capacitance dilatometer was utilized, which allows a very accurate study of crystal length changes. We measured the macroscopic length changes dL/L of polycrystalline samples. The linear thermal expansion coefficient α was calculated as the first temperature derivative of dL/L, while the volume thermal expansion coefficient is given by $\beta_{\rm vol} = 3\alpha$ for our polycrystalline samples. The specific heat was studied in a Quantum Design PPMS calorimeter by means of a relaxation technique. In the electrical transport experiments the samples were investigated by four-probe ρ measurements using an alternating DC-current. The ESR measurements at a frequency of $\nu = 9.6\,\mathrm{GHz}$ were carried out in a standard Bruker EMX system. The HF-ESR experiments were performed with a home-made spectrometer[16] at frequencies $\nu = 83 - 348\,\mathrm{GHz}$ and magnetic fields $B = 0 - 15\,\mathrm{T}$. All ESR measurements were made in a temperature range of $5 - 300\,\mathrm{K}$.

B. Sample preparation

The polycrystalline samples $GdO_{1-x}F_xFeAs$ ($x = 0, 0.15, 0.17$, nominal content) were prepared by two different routes. Route 1, which is similar to that described in Ref. [17], starts with FeAs, Gd, Gd_2O_3 and GdF_3 in a stoichiometric ratio. All materials were homogenized by grinding in a mortar. Route 2 uses GdAs, Fe, Fe_2O_3 and FeF_3 as starting materials in a stoichiometric ratio. Here, the starting materials were homogenized by grinding in a ball mill. In either case, the resulting powders were pressed into pellets under Ar atmosphere, and subsequently annealed in an evacuated quartz tube either in a two step synthesis at 940°C for 12 h and at 1150°C for 48 h (60 h) or in a one step synthesis at 940°C for 168 h. In order to confirm the single phase character of the polycrystals, powder x-ray diffraction was performed on a Rigaku diffractometer (Cu K_α-radiation, graphite monochromator). The samples were either phase pure or contained insignificantly small amounts of GdAs, GdOF, and Fe_3O_4. The microstructure and the composition were examined by scanning electron microscopy (SEM, XL30 Philipps, IN400) equipped with an electron microprobe analyzer for semi-quantitative elemental analysis using the wave length dispersive x-ray (WDX) mode. The analysis showed that the sample with $x = 0.15$ (nominal content) in fact contains $\sim 0.07 \pm 0.02$ of F and $x = 0.17$ contains $\sim 0.14 \pm 0.02$ of F. Further on, we will use the doping levels obtained by WDX in order to label the samples.

For the c-axis alignment of the parent GdOFeAs sample, which was synthesized under high pressure[18], the powder was mixed with epoxy resin and hardened while rotating in a magnetic field of 1.5 T. The x-ray diffraction data of the aligned powder samples were collected at room temperature using a PANalytical X'Pert PRO system (Philips) with Co K_α-radiation (Fig. 1). The presence of highly intense [00l] reflections (Fig. 1, arrows) which dominate the pattern points to a sufficiently good quality of the alignment. Reflections with Miller indices different from [00l] (Fig. 1, asterisks) are visible in the background, too, but their intensity is strongly suppressed compared to the powder pattern.

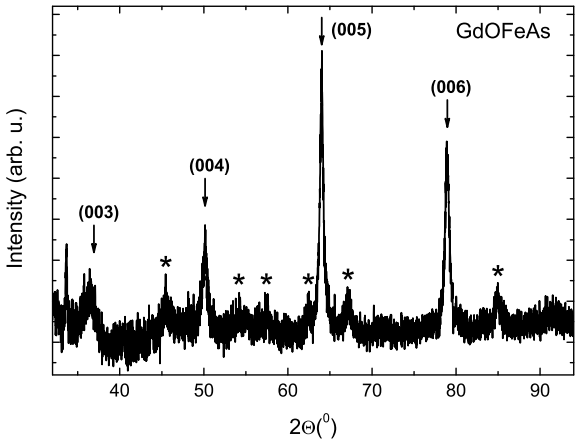

FIG. 1: Powder x-ray diffraction data of the c-axis aligned GdOFeAs sample.

III. THERMODYNAMIC AND TRANSPORT MEASUREMENTS

In Fig. 2(a), the temperature dependence of the static susceptibility $\chi = M/B$ of GdOFeAs is presented. As $\chi(T)$ is dominated by the response of the Gd moments, the results are very similar for the F-doped samples, which are not shown. In general, the data obey the Curie-Weiss law which is expected due to the presence of paramagnetic Gd^{3+} ions. Note that the response of the FeAs-layers which is e.g. visible in LaOFeAs is about 3 orders of magnitude smaller and hence masked by the magnetism of the rare earth ions.[19] The linear temperature dependence of the inverse susceptibility demonstrates the Curie-Weiss-like behavior. Analyzing the data in terms of the Curie-Weiss-law yields the antiferromagnetic Weiss temperature $\Theta = -16 \pm 1\,\mathrm{K}$ and the effective magnetic moments $p_{\rm eff} = 7.81 \pm 0.04\,\mu_{\rm B}$ which is close to the magnetic moment of a free Gd^{3+} ion ($p_{\rm eff} = 7.94\,\mu_{\rm B}$). At a low temperature of about $\sim 5\,\mathrm{K}$ there is a kink of the magnetization due to the AFM ordering of the Gd moments.

While the structural and Fe magnetic phase transitions are not visible in the magnetization data, there are pronounced anomalies in the specific heat $c_{\rm p}$ and the thermal

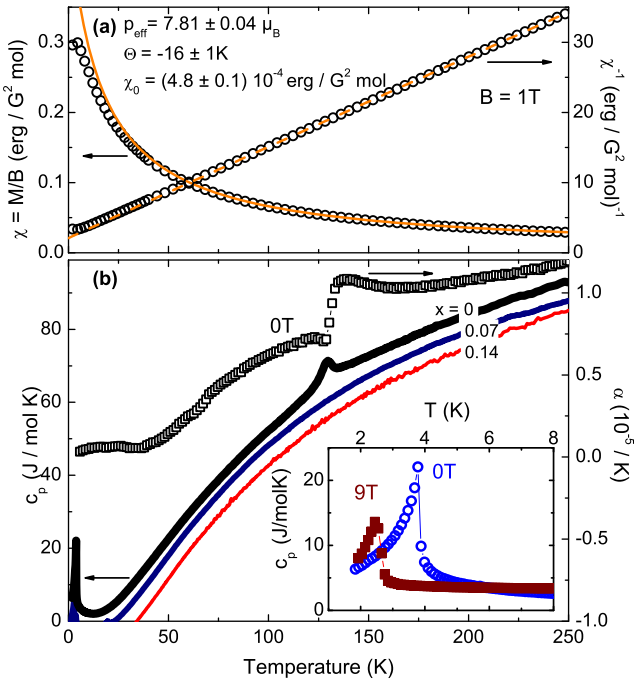

FIG. 2: (Color online) **(a)** Static susceptibility $\chi = M/B$ (left axis), χ^{-1} (right axis); **(b)** specific heat c_p (left axis) and thermal expansion coefficient α (right axis) of GdOFeAs vs. temperature; specific heat data for $x = 0.07$ and $x = 0.14$ samples is artificially shifted down for clarity; inset in **(b)** panel presents specific heat anomaly associated with long-range antiferromagnetic ordering of the Gd-moments at $B = 0$ and $B = 9$T.

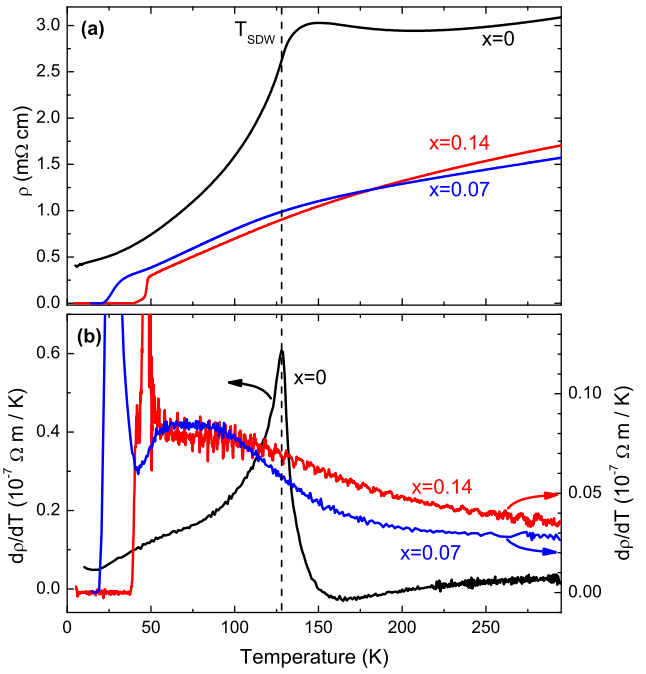

FIG. 3: (Color online) **(a)** Electrical resistivity ρ of $GdO_{1-x}F_xFeAs$ samples, $x = 0$, 0.07, 0.14; **(b)** electrical resistivity derivative dρ/dT for $x = 0$ (left axis), $x = 0.07$, 0.14 (right axis).

expansion coefficient α (Fig. 2(b)) in the case of the parent GdOFeAs sample. There is one broad feature visible in the specific heat data. In contrast, the thermal expansion coefficient exhibits two huge anomalies with opposite sign which can be attributed to the structural and SDW transitions of the compound at $T_{ST} = 136 \pm 5$ K and $T_{SDW} = 128 \pm 2$ K. In addition, the specific heat data reveal a sharp anomaly at $T_{\mathrm{N^{Gd}}} = 3.8$ K which is associated with the onset of long range antiferromagnetic order of the Gd moments, in accord with the magnetization data. Note that the anomaly is not present in our thermal expansion data due to the restricted temperature range $T \geq 6$ K. Upon application of external magnetic fields, Gd order is strongly suppressed as shown in Fig. 2 (inset in the lower panel). $T_{\mathrm{N^{Gd}}}$ is shifted to 2.5 K in an external magnetic field of $B = 9$ T. While anomalies associated with Gd-ordering are still observed in the specific heat data of the F-doped samples with $x = 0.07$ and $x = 0.14$, there are no visible anomalies at higher temperatures (Fig. 2(b)). This evidences the absence of long-range SDW order in the doped, superconducting samples.

Fig. 3(a) shows the temperature dependence of the electrical resistivity ρ of the $GdO_{1-x}F_xFeAs$ samples for all three doping levels: $x = 0$, 0.07 and 0.14. To get a better insight into the data we present the temperature derivatives $d\rho/dT$ in the bottom panel (Fig. 3(b)). The resistivity of the undoped material exhibits features closely connected to the structural and magnetic phase transitions: a maximum close to T_{ST} and an inflection point at $T_{SDW} = 128$ K, which are characteristic for all the 1111 parent compounds[4,17,20]. With doping, the electrical resistivity drastically changes its behavior, superconductivity emerges at low temperature and the intermediate temperature maximum disappears. The SC temperatures T_c for $x = 0.07$ and $x = 0.14$ samples amount to 20 K and 45 K, respectively. No pronounced features of the SDW phase are present in these compounds in the whole investigated temperature range. However, the normal state behavior of $\rho(T)$ for $x = 0.07$ is very unusual. At high temperatures the resistivity is linear down to approx 200 K, then it develops a curvature and drops below the linear approximation of the high temperature part. With decreasing temperature further, $\rho(T)$ becomes linear again and develops a slight opposite curvature at $T \lesssim 50$ K, prior to the onset of superconductivity. Upon increasing the F doping level in the samples, namely to $x = 0.14$, this anomaly becomes weaker. A similar drop of $\rho(T)$ at $T \lesssim 200$ K as found here has previously been observed for other 1111-type pnictide superconductors[4,17,21] as well as for $Ba_{1-x}K_xFe_2As_2$[22,23]. The qualitative resemblance to the sharp drop at T_{SDW} which is observed in the respective parent compounds suggests that the resistivity drop in the superconducting samples is indicative of remnants of the SDW phase. In fact, a recent study of the Nernst

effect on $LaO_{1-x}F_xFeAs$ provides strong evidence that precursors of the SDW phase develop in the vicinity of the resistivity anomaly despite the absence of static magnetism[24].

IV. ELECTRON SPIN RESONANCE, RESULTS AND DISCUSSION

A. GdOFeAs, 9.6 GHz X-band measurements

The ESR measurements performed at a frequency of 9.6 GHz on the c-axis aligned GdOFeAs sample in the whole temperature range of study and for both sample orientations (H_{ext} || or ⊥ c) reveal one broad line with the g-factor ∼ 2 (Fig. 4(a), inset). Such ESR response is typical for the systems where Gd^{3+} ions occupy regular positions in the crystal lattice with short distances between neighboring ions[25]. The Gd^{3+} is an S-state ion with a half-filled $4f$ shell which yields an isotropic g-factor equal to 2 and a spin value of 7/2. The rather big spin value leads to strong magnetic dipole-dipole interactions which together with the unresolved fine structure broaden the ESR line. This broadening mechanism should lead to a gaussian line shape which is however not observed in the spectra. Instead, the lorentzian[38] function had to be used to fit the spectra (thin line in the inset in Fig. 4(a)) in order to obtain accurate values of the resonance field (H_{res}) and the linewidth. The lorentzian shape suggests that homogeneous narrowing of the line does take place, which can be caused by isotropic exchange interaction between Gd spins[25,26]. The temperature dependencies of H_{res} and the linewidth are shown on Fig. 4(a),(b). With lowering the temperature no drastic changes are seen in H_{res} down to ∼ 10 K where there is a strong shift of the line due to the ordering of Gd moments (Fig. 4(a)). The linewidth, in contrast to the resonance field, shows clear change in the behavior at $T_{SDW} = 128$ K for both sample orientations (Fig. 4(b)). At temperatures above T_{SDW} there is a gradual decrease of the width of the ESR line upon cooling. This can be attributed to a Korringa-like behavior, with the linewidth having a linear in T contribution due to the relaxation of the Gd spins through interaction with the conduction electrons, similar to $EuFe_2As_2$[27]. The slope value amounts to $\sim 0.9 \cdot 10^{-4}$ T/K which is one order of magnitude smaller than that in $EuFe_2As_2$. A strong broadening of the line below T_{SDW} can be attributed to the formation of the SDW state in the FeAs layers. Similar effects in the Gd^{3+} ESR linewidth were observed before in the case of Gd_2BaCuO_5 samples where exchange coupling of Gd- and Cu-moments enabled to probe by means of Gd^{3+} ESR the magnetic ordering of the Cu layers[28] (see the discussion below).

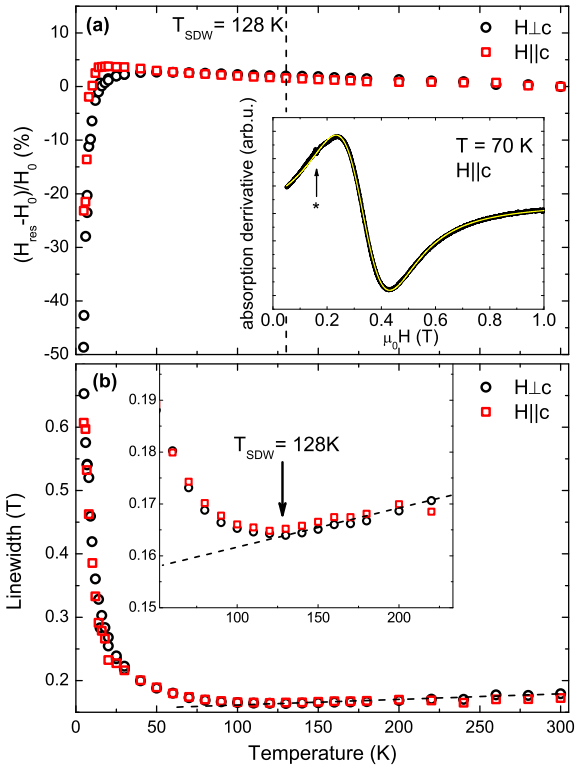

FIG. 4: (Color online) Results of the X-Band ESR (ν = 9.6 GHz) measurements performed on c-axis aligned powder GdOFeAs sample for two sample orientations in the magnetic field, open circles - field in ab plane, open squares - field parallel to the c-axis; **(a)** temperature dependence of the resonance field on a reduced field scale $(H - H_0)/H_0$. Here $\mu_0 H_0 = 0.323/0.328$ T is resonance field at the highest temperature for $H \perp c/H \parallel c$; the inset shows the spectrum at $T = 70$ K in $H \parallel c$ configuration, the arrow points at a small Fe ESR signal which presence indicates a small amount of impurities; **(b)** temperature dependence of the linewidth; inset shows the change of the T-dependence at the SDW transition

B. GdOFeAs, high-frequency/field measurements

In the measurements performed at 9.6 GHz, the linewidth of the Gd^{3+} ESR signal is comparable to its resonance field. This leads to complications in the spectra analysis and to a lack of resolution. In order to improve the spectral resolution we performed high-frequency/field measurements on GdOFeAs samples. The high-temperature ESR spectra of the non-oriented GdOFeAs powder sample measured at a frequency of 328 GHz (Fig. 5(a)) consist of a single broad lorentzian-shaped line with a g-factor of ∼ 2 and a linewidth of ∼ 0.2 T, similar to the low-frequency measurements. However, the very small Korringa contribution detected in the low frequency measurements is not visible in the HF-ESR spectra (Fig. 9a). The low-temperature HF-ESR spectra exhibit an inhomogeneously broadened shape which is in contrast to X-band data. As a measure of this broadening the full width at

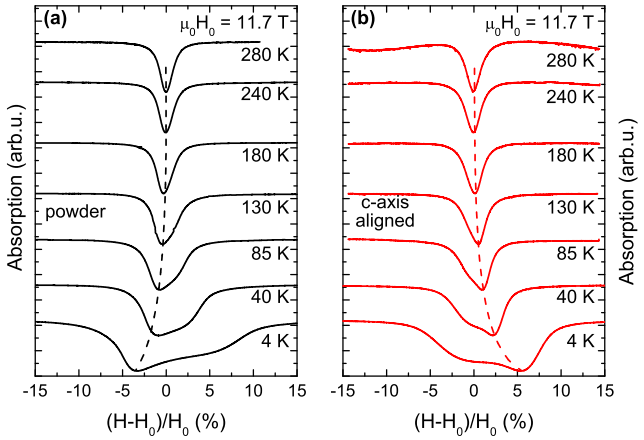

FIG. 5: (Color online) Temperature evolution of the high-frequency/field ESR spectra of GdOFeAs powder and c-axis aligned powder samples at a frequency of $\nu = 328\,\mathrm{GHz}$, shown on a reduced field scale $(H - H_0)/H_0$. Here $\mu_0 H_0 = 11.7\,\mathrm{T}$ is the resonance field of the signal at high temperature; **(a)** non-oriented powder; **(b)** c-axis oriented powder.

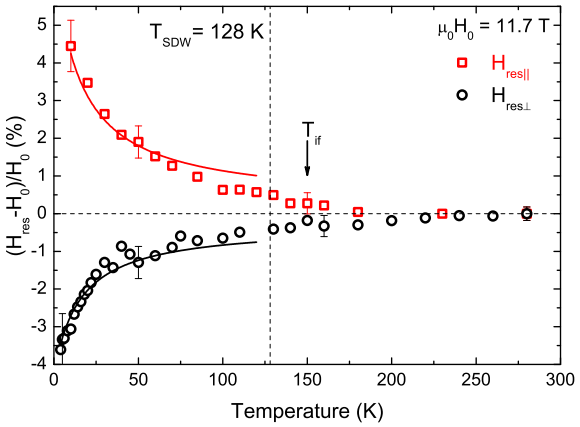

FIG. 6: (Color online) The shift of the minimum of absorption of the spectra with temperature, measured at a frequency of $\nu = 328\,\mathrm{GHz}$, on a reduced field scale $(H_{res} - H_0)/H_0$. Here $\mu_0 H_0 = 11.7\,\mathrm{T}$ is the resonance field of the signal at high temperature; open circles - powder sample, open squares - c-axis aligned powder sample, solid lines - fits of the resonance field using Eq. A.4.

the half maximum (FWHM) of the signal ΔH has been taken (see Fig. 9(a)). As can be seen, with decreasing the temperature there is only a weak broadening of the signal down to a characteristic temperature $T_{if} \sim 150\,\mathrm{K}$ (if denotes an internal field at the Gd ion, see the discussion below) where substantial inhomogeneous broadening begins to develop continuously down to the lowest measured temperature of 4 K. Concomitantly with the inhomogeneous broadening there is a noticeable shift of the minimum of the absorption to lower fields, as shown on Fig. 6 (open circles) on a reduced field scale $(H - H_0)/H_0$. Here $\mu_0 H_0 = 11.7\,\mathrm{T}$ is the resonance field of the signal at high temperature. The spectral shape at low temperature (Fig. 5(a)) appears to be very similar to the shape of the ESR signal from a powder sample with an anisotropic g-factor. However, since the Gd^{3+} ion is a pure S-state ion, it should have an isotropic g-factor very close to 2. Hence one can conjecture that the shape of the ESR signal from the GdOFeAs sample is caused by the anisotropy of the internal field at the Gd site arising from the AFM-ordered Fe moments. In such an anisotropic powder situation most of the spectral weight is coming from the grains whose c-axes are oriented perpendicular to the direction of the external field H_{ext}. One should note here that in the case of in-plane anisotropy there will be an additional averaging effect due to the distribution of resonance fields of grains whose (ab)-planes are parallel to H_{ext}. Therefore we assume here that the low-field minimum of the absorption corresponds to the mean value of the resonance field of the Gd^{3+} ESR response ($H_{res\perp}$) in the case of the external field applied perpendicular to the c-axis. Correspondingly, the high-field shoulder of the spectra arises from grains whose c-axes make small angles with respect to H_{ext}.

In order to probe the Gd^{3+} response for the geometry $H_{\mathrm{ext}} \parallel c$ we have performed ESR measurements on the c-axis oriented GdOFeAs powder sample. Though, according to the x-ray diffraction analysis, the alignment of the powder particles was not perfect, a substantial c-axis texturing of the sample has been achieved (Fig. 1). Similarly to the non-oriented powder sample, the c-axis oriented sample at temperatures above $\sim 150\,\mathrm{K}$ exhibits only a small broadening of the ESR spectrum with decreasing temperature (Fig. 5(b)). Below this temperature the signal experiences strong inhomogeneous broadening where most of the spectral weight is shifted to higher fields, which is opposite to the finding in the non-oriented powder sample. In the oriented sample most of the spectral weight and, consequently, the minimum of the absorption should correspond to the resonance field of the Gd^{3+} ESR response ($H_{res\parallel}$) in the geometry $H_{ext} \parallel c$ whereas a non-ideal powder alignment yields the low-field shoulder of the ESR signal.

From our measurements on non-oriented and c-axis oriented powder samples one can, therefore, extract the temperature dependencies of H_{res} in two configurations, i.e., for fields aligned along the c-axis ($H_{res\parallel}$) and in the (ab)-plane ($H_{res\perp}$), as summarized in Fig. 6. As can be seen, the changes of both resonance fields $H_{res\perp}$ and $H_{res\parallel}$ start upon cooling at $T_{if} \lesssim 150\,\mathrm{K}$ and the shifts have opposite directions.

The qualitative difference in the high-field/frequency and low-field/frequency measurements leads to the conclusion that the shift of the resonance field and the inhomogeneous broadening of the spectra measured at a frequency of 328 GHz is a field-induced effect. To investigate it, we have measured the frequency ν versus magnetic field H_{res} dependence of the GdOFeAs powder and the c-axis aligned samples, respectively, both at $T = 280\,\mathrm{K}$ and $T = 4\,\mathrm{K}$ (Fig. 7). At $T = 280\,\mathrm{K}$ the spectrum at all studied frequencies and fields consists of

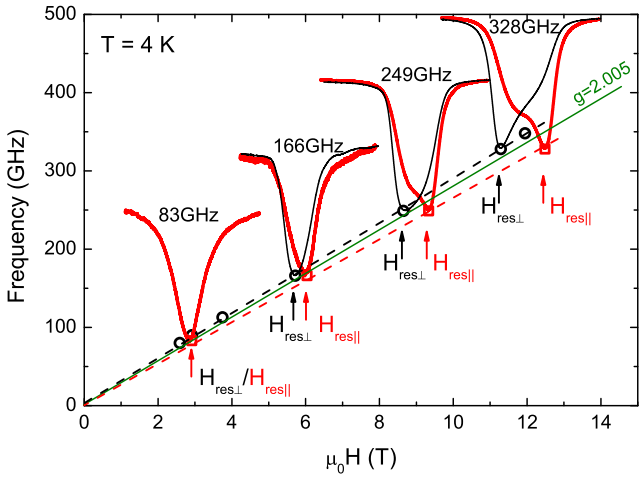

FIG. 7: (Color online) Frequency dependence of the ESR signal from GdOFeAs non-oriented powder and c-axis oriented powder samples measured at $T = 4\,\mathrm{K}$; data points correspond to the position of the minimum of absorption of the spectra at different frequencies, open circles - non-oriented powder sample, open squares - c-axis oriented powder sample, dashed lines - guides for the eyes, solid line - the frequency dependence of the position of the high-T Gd ESR line measured at $T = 280\,\mathrm{K}$; the lineshape of the spectra is shown as well, thin solid line - non-oriented powder, thick solid line - c-axis oriented powder.

a single lorentzian line with the same linewidth value. A linear $\nu(H_{res})$ dependence has been revealed yielding a g-factor $g = h\nu/(\mu_B H_{\mathrm{res}})$ equal to 2.005 (straight solid line on Fig. 7). The spectra at $T = 4\,\mathrm{K}$ for the non-oriented powder (thin line) and c-axis oriented powder (thick line) samples at different frequencies together with the frequency dependence of the resonance fields $H_{res\perp}$ and $H_{res\parallel}$ are shown on Fig. 7 as well. This measurement reveals that the difference between $H_{res\perp}$ and $H_{res\parallel}$ increases linearly with increasing the frequency and the field strength.

C. GdOFeAs, discussion

Since the inhomogeneous broadening and the shift of the Gd ESR signal set in close to the SDW ordering temperature, one can associate them with the interaction of the Fe ordered moments with the Gd spins. The shifts of $H_{res\perp}$ and $H_{res\parallel}$ from a common high-temperature paramagnetic value H_0 can hence be related to the occurrence of an internal magnetic field ($H_{int\perp}$ and $H_{int\parallel}$) at the Gd site due to the formation of the static SDW in the FeAs layer. Based on the dependence shown on Fig. 7 we can conclude that the strength of these internal fields depends on the strength of the applied magnetic field.

When the FeAs planes are in the paramagnetic state, at temperatures above $T_{SDW} = 128\,\mathrm{K}$, the exchange/dipolar field at the Gd position is negligible as the applied magnetic field cannot effectively polarize small paramagnetic moments at elevated temperatures. At temperatures below $T_{SDW} = 128\,\mathrm{K}$ the Fe moments order *statically* in the (ab)-plane. The AFM structure of the magnetic order, which is similar for all R-based 1111-type pnictides can be found in Ref. 15. Due to symmetry reasons, without an applied magnetic field the internal field at the Gd site can be only of dipolar nature and in this case according to an estimate it should not exceed $\sim 0.03\,\mathrm{T}$. We suggest that application of an external magnetic field induces tilting of the Fe spins and hence creates an uncompensated magnetic moment (m_{Fe}) in the direction of the external field[39]. This moment can interact with the Gd^{3+} spins which would effectively lead to the occurrence of an additional internal field. If $H_{ext} \perp c$, then the Fe spins tilt in the ab plane as it is schematically shown on Fig. 8(a,b) for the configuration where H_{ext} makes an angle of 90° with the AFM ordered Fe spins. The shift of the ESR line $H_{res\perp}$, measured at 328 GHz, yields an estimate of the internal field ($H_{int\perp}$) of about $\approx 0.4\,\mathrm{T}$ parallel both to H_{ext} and to the uncompensated moment m_{Fe} in the FeAs plane. If $H_{ext} \parallel c$, then the Fe moments tilt out of the plane (Fig. 8(c,d)). In this case the shift of the ESR line, measured at 328 GHz, yields an estimate of the internal field ($H_{int\parallel}$) of about $\approx 0.65\,\mathrm{T}$ antiparallel both to the H_{ext} and to the uncompensated moment m_{Fe}. One should note here that an estimate of the dipolar field produced by the FeAs layers at the Gd site yields a value which does not exceed $\approx 0.05\,\mathrm{T}$ even for full out-of-plane canting. This field is one order of magnitude smaller than the experimentally observed value which clearly implies the presence of an appreciable exchange interaction between Gd and canted Fe moments. The dependence of the sign of the internal field on the direction of the applied magnetic field suggests that the sign of the exchange interaction with Gd spins is different for different directions of the uncompensated Fe moments, i.e., ferromagnetic for the in-plane and antiferromagnetic for the out-of-plane directions. This surprisingly strong anisotropy of the exchange might be related with the multiband electronic structure of iron pnictides which might give rise to different pathways for interactions between the Gd $4f$ orbitals and the in-plane xy and out-of-plane xz and yz Fe $3d$ bands. Note that, in zero magnetic field and hence without Fe spin canting ($m_{Fe} = 0$), the exchange interaction between Fe and Gd moments of an arbitrary sign is geometrically frustrated (see Fig. 8). The application of a field which tilts the Fe moments thus removes this frustration.

Considering the exchange interaction, one might suppose that the temperature dependence of the internal field at the Gd site should follow the behavior of the SDW order parameter in 1111 compounds[6,15,29], which increases fast within $\sim 30\,\mathrm{K}$ starting at T_{SDW} and then stays almost constant with further decreasing the temperature. Here, the internal field acting on the Gd^{3+} moments arises at a temperature $T_{if} \approx 150\,\mathrm{K}$ which is $\sim 20\,\mathrm{K}$ higher than $T_{SDW} = 128\,\mathrm{K}$ and keeps increasing upon cooling till the lowest measured temperature

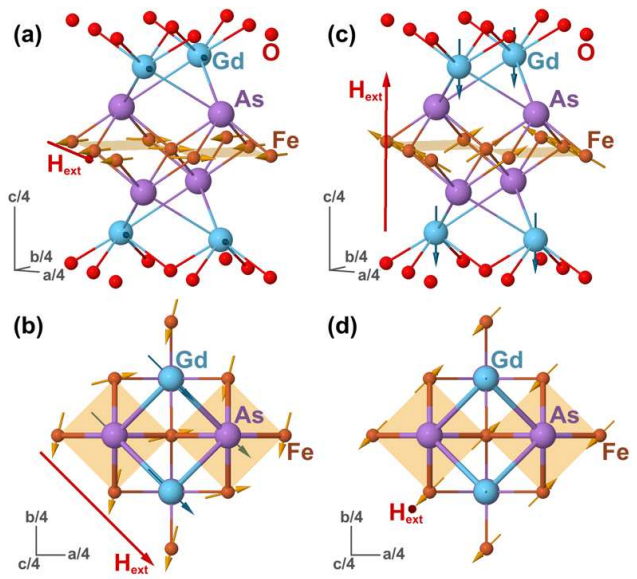

FIG. 8: (Color online) Canting of the Fe moments due to the applied magnetic field H_{ext}; **(a),(b)** $H_{ext} \perp c$ (angle between H_{ext} and Fe AFM ordered moments is 90°); **(c),(d)** $H_{ext} \| c$; arrows on the Fe site depict magnetic moments, whereas arrows on the Gd sites represent the induced internal field.

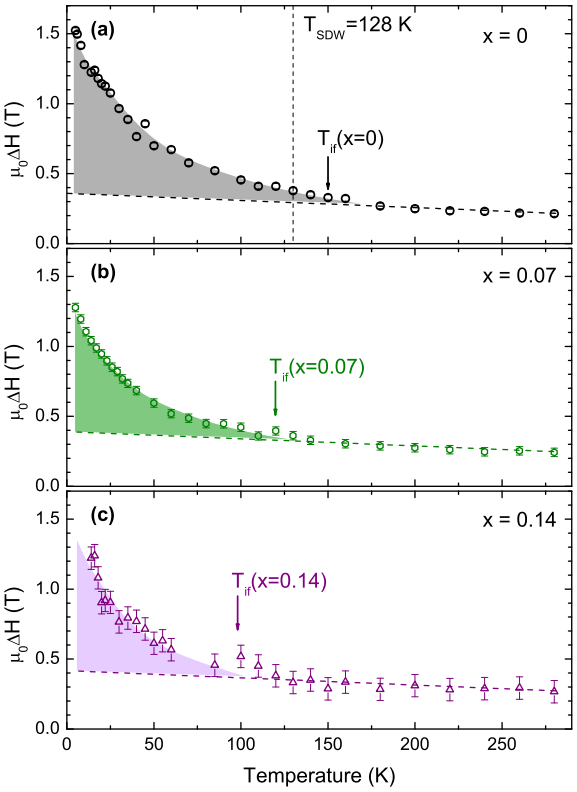

FIG. 9: (Color online) The full width at the half maximum (FWHM) ΔH of the ESR lines, measured at a frequency of $\nu = 348$ GHz ($x = 0.07$) and $\nu = 328$ GHz ($x = 0, 0.14$), as a function of temperature for the non-oriented $GdO_{1-x}F_xFeAs$ samples; **(a)** $x = 0$; **(b)** $x = 0.07$; **(c)** $x = 0.14$.

(see Fig. 6). When approaching the temperature of the SDW transition from high temperatures, the appearance of the internal field well above T_{SDW} can be explained by growing quasi-static correlations between the Fe moments seen in the time window of the high-frequency ESR. The development of the internal field below T_{SDW} is found to be similar to that of some other systems where paramagnetic ions are coupled to magnetically-ordered moments of another type[30,31]. To explain this evolution of the internal field we use a simple model based on a mean-field approximation[25,32] (for details see Appendix). According to this model the internal field depends on the applied magnetic field and on temperature as following (see Eq. A.5):

$$H_{int} \sim \pm \frac{A(J, \alpha, C_{Gd}) H_{ext}}{(T - \Theta)}$$

Here $A(J, \alpha, C_{Gd})$ is a parameter determined by the Gd-Fe exchange coupling energy J, by the susceptibility of the ordered Fe moments to the applied field α and by the Gd Curie constant C_{Gd}. As can be seen, this dependence qualitatively obeys a Curie-Weiss law at a given applied field which agrees well with the measured data. The model enables to fit the experimental data points reasonably well (see Appendix and Fig. 6). Firstly, the fit yields an estimate of the energy of the exchange coupling between Gd and Fe spins which is in the range of $|J| \approx 15 - 20$ K. Secondly, it shows that the magnitude of the uncompensated Fe moment depends on the Gd magnetization which suggests that the Gd subsystem additionally tilts or polarizes the SDW.

To summarize this part, the ESR results on GdOFeAs samples show that the Gd subsystem is exchange-coupled to the magnetic FeAs planes. On approaching the AFM SDW transition from above, the growing correlations between the Fe moments yield a shift of the Gd ESR line. At lower temperature, depending on the angle between H_{ext} and the c-axis of the sample, the signal shifts to higher or to lower fields due to the uncompensated exchange field which is transferred to the Gd site from the Fe moments canted in an external magnetic field. Since the full width at the half maximum ΔH is proportional to the difference between resonance fields $H_{res\perp} - H_{res\|}$, then the width of the ESR signal ΔH of the non-oriented powder sample can be taken as a measure of this exchange field (Fig. 9a).

D. $GdO_{1-x}F_xFeAs$ ($x = 0.07$, 0.14)

The influence of the fluorine doping on the Gd ESR has been studied on two powder samples of $GdO_{1-x}F_xFeAs$ with 7% and 14% of fluorine. On Fig. 10(a),(b) the evolution of the respective Gd^{3+} ESR spectra is shown on a reduced field scale. Similarly to the undoped sample, at high temperature the ESR spectrum for both doped

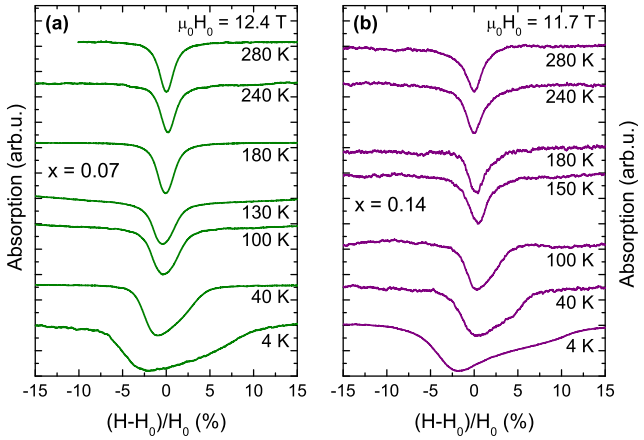

FIG. 10: (Color online) Temperature evolution of the high-frequency/field ESR spectra of $GdO_{1-x}F_xFeAs$ powder samples measured at a frequency of $\nu = 348\,\mathrm{GHz}$ ($x = 0.07$) and $\nu = 328\,\mathrm{GHz}$ ($x = 0.14$), shown on a reduced field scale $(H - H_0)/H_0$. Here H_0 is the resonance field of the signal at high temperature; **(a)** $x = 0.07$, $\mu_0 H_0 = 12.4\,\mathrm{T}$; **(b)** $x = 0.14$, $\mu_0 H_0 = 11.7\,\mathrm{T}$.

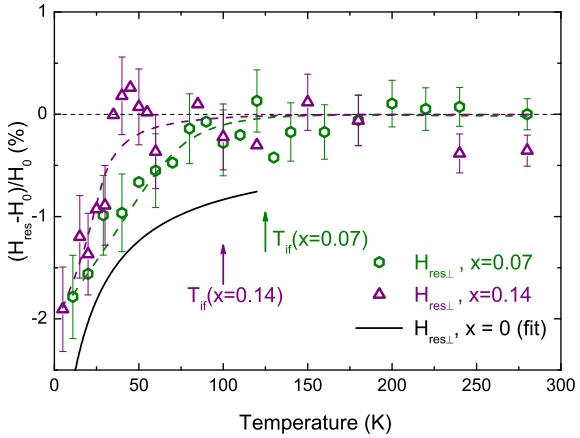

FIG. 11: (Color online) The shift of the minimum of absorption of the spectra with temperature, measured at a frequency $\nu = 348\,\mathrm{GHz}(x = 0.07)/328\,\mathrm{GHz}(x = 0.14)$, on a reduced field scale $(H_{res} - H_0)/H_0$. Here $\mu_0 H_0 = 12.4\,\mathrm{T}/11.7\,\mathrm{T}$ is the resonance field of the signal at high temperature, open hexagons - $x = 0.07$, open triangles - $x = 0.14$, solid line - fit of the resonance field in the parent GdOFeAs sample.

samples consists of a single lorentzian-shaped line with $g = 2.005$. While lowering the temperature, the line remains almost unchanged until a characteristic temperature T_{if} is reached. This temperature corresponds to the onset of an additional inhomogeneous contribution to the width of the ESR signal ΔH. This inhomogeneous contribution is shown by the shaded area on Fig. 9(b,c). The temperature T_{if} clearly depends on the fluorine doping level. In the case of the 7% F-doped sample a noticeable broadening of the line starts at $T_{if}(x = 0.07) \sim 125\,\mathrm{K}$, whereas for the 14% doped sample it starts at a lower temperature $T_{if}(x = 0.14) \sim 100\,\mathrm{K}$. For both doped

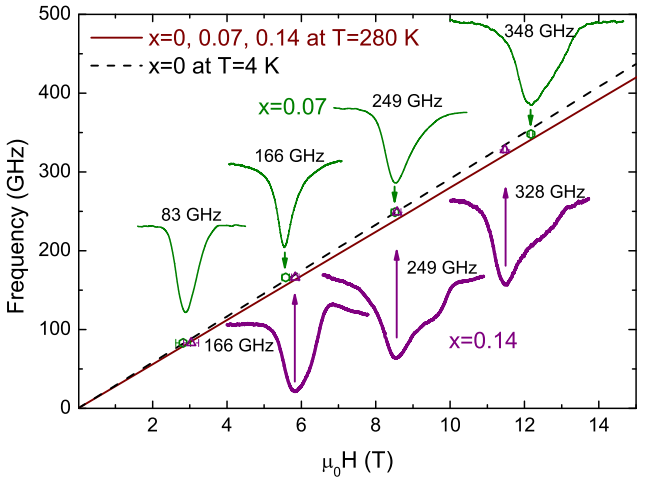

FIG. 12: (Color online) Frequency dependence of the ESR signal from $GdO_{1-x}F_xFeAs$ powder samples measured at a temperature of $T = 4\,\mathrm{K}$, in SC state; data points correspond to the position of the minimum of absorption of the spectra at different frequencies, open hexagons - $x = 0.07$, open triangles - $x = 0.14$, dashed line - guide for the eyes, solid line - the frequency dependence of the position of the high-T Gd ESR line measured at $T = 280\,\mathrm{K}$ for both F-doped samples; the lineshape of the spectra is shown as well, thin solid line - $x = 0.07$, thick solid line - $x = 0.14$.

samples there is a shift of the minimum of the absorption ($H_{res\perp}$) to lower magnetic fields below T_{if} (Fig. 11). Qualitatively this shift is similar to that of the undoped sample (solid line on Fig. 11), but it is less pronounced. In addition, the inhomogeneous broadening and the shift of $H_{res\perp}$ to lower magnetic fields exhibit a magnetic field dependence similar to that of the undoped GdOFeAs sample (Fig. 12).

E. Superconducting $GdO_{1-x}F_xFeAs$, discussion

The remarkable similarities of the Gd ESR behavior between the fluorine-doped samples and the undoped one strongly suggest that, even in the superconducting samples where the phase transition to the AFM SDW state is not observed in the thermodynamics and transport properties, quasi static (on the time scale of the ESR measurement) magnetic correlations in the FeAs planes are present below the characteristic temperature T_{if}. Such correlations may explain the peculiar features in the resistivity data shown in Sec. III.

The unified phase diagram for the iron pnictides, especially for the 1111 materials, is not fully established so far since the issue of coexistence of superconductivity and magnetism remains controversial. The nonmagnetic rare earth based $LaO_{1-x}F_xFeAs$ material exhibits no evidence for the presence of a static magnetic order for any superconducting composition, but rather reveals SDW-like spin fluctuations seen in the transport[24] and inelastic

neutron scattering experiments[33,34]. On the other hand, the *magnetic* rare earth based systems (Sm, Nd, Ce) studied so far demonstrate coexistence of superconductivity and static magnetism at least in the underdoped region[3,11]. Our high-field ESR results show that there is yet another 1111 system comprising a strongly magnetic rare earth (Gd) subsystem where the coexistence of quasi-static magnetism and superconductivity is still visible in large doping range. Here, the increase of the fluorine content and correspondingly the rise of T_c leads to the suppression of magnetic correlations indicating a possible interplay between these two states. All this suggests that the coexistence and possible interplay of the static or quasi-static magnetism and superconductivity may be a generic property of 1111-type compounds. In this regard, a remaining question yet to be answered is the extent to which the R-Fe magnetic interaction influences the magnetic correlations in the FeAs planes. Moreover, the issue of the coexistence of magnetism and superconductivity is frequently discussed in the literature for other pnictide families as well. Extending ESR experiments to compounds of these families would be of great interest.

V. CONCLUSION

Our HF-ESR study of polycrystalline samples of the $GdO_{1-x}F_xFeAs$ superconductor reveals a magnetic coupling between the Gd subsystem and the FeAs layers. This coupling, most probably of the anisotropic exchange type, is visible in the Gd ESR response in the undoped GdOFeAs in the SDW state, in form of a field-induced inhomogeneous broadening and shift of the ESR spectrum. This effect is caused by the interaction of the Gd spins with the uncompensated Fe moments due to the canting of the Fe moments in magnetic field. Furthermore, the data suggest that the Gd moments additionally tilt the ordered Fe moments. Surprisingly, the broadening and the shift of the spectrum are present also in the doped superconducting samples where there is no evidence of long range magnetic order. This points to the presence of short range, static on the ESR time scale, magnetic correlations. This may be relevant to the interplay of magnetism and superconductivity in these materials, where on doping with fluorine there is a simultaneous increase of the superconducting critical temperature and suppression of the magnetic correlations. The possible relevance of the exchange interaction between the magnetic rare-earth subsystem and the FeAs planes to the properties of this novel class of superconductors remains to be elucidated.

Acknowledgments

We thank S. Müller-Litvanyi, R. Müller, J. Werner, and S. Pichl for assistance in the sample preparation. We thank U. Stockert and J. E. Hamann-Borrero for assistance in the sample characterization. The work at the IFW Dresden was supported by the Deutsche Forschungsgemeinschaft through Grants No. BE1749/12 and BE1749/13, the Research Unit FOR538 (Grant No. BU887/4) and the Priority Programme SPP1458 (Grant No. GR3330/2). Work at the ETH was supported by the Swiss National Science Foundation through the National Center of Competence in Research MaNEP (Materials with Novel Electronic Properties).

Appendix

Here we provide a calculation of the internal field on the Gd ion using a simple model based on the mean-field approximation[25,32]. To simplify the calculations we assume that a magnetic field and magnetic moment vectors are collinear. In this model, the internal field at the Gd site H_{int} is proportional to the magnitude of the uncompensated Fe moment m_{Fe} with a coefficient λ:

$$H_{int} = \pm\lambda m_{Fe} \tag{A.1}$$

Hereafter the sign depends on the type of interaction, being "+" for ferromagnetic and "−" for antiferromagnetic exchange. Neglecting the weak dipolar contribution, the magnetization normalized to the single ion m_{Gd} of the Gd subsystem is proportional to the sum of the applied magnetic field H_{ext} and internal field H_{int}:

$$m_{Gd} = \chi_{Gd}(T)\,(H_{ext} \pm H_{int}), \tag{A.2}$$

where $\chi_{Gd}(T) = C_{Gd}/(T-\Theta)$ is the Gd magnetic susceptibility, C_{Gd} is the Gd Curie constant, Θ is the Gd Curie temperature. Due to the exchange interaction, the uncompensated magnetic moment m_{Fe} is proportional not only to the applied field but also to the internal field created by the Gd moments:

$$m_{Fe} = \alpha(H_{ext} + \lambda m_{Gd}) \tag{A.3}$$

Here α is the susceptibility of the ordered Fe moments to the external magnetic field. Using Eq. A.1, Eq. A.2 and Eq. A.3 one can obtain the equation for the internal field H_{int} at the Gd site:

$$H_{int} = \pm\frac{\lambda^2\alpha C_{Gd} + \lambda\alpha(T-\Theta)}{(T-\Theta) - \lambda^2\alpha C_{Gd}} H_{ext} \tag{A.4}$$

Eq. A.4 enables to fit the measured temperature dependence of the internal field (see Fig. 6). The resonance field of the Gd is determined by the applied field and by the internal field $H_0 = H_{ext} \pm H_{int}$. At high temperatures when there is no internal field at the Gd site at any strength of the applied magnetic field ($H_{int} = 0$) one can measure the resonance field $H_0 = 11.7\,\mathrm{T}$ (for measurement frequency $\nu = 328\,\mathrm{GHz}$). Assuming that the resonance field of the Gd ions $H_0 = 11.7\,\mathrm{T}$ stays constant at all measured temperatures one obtains the expression for

the applied field $H_{ext} = H_0 \mp H_{int}$ ($H_0 = 11.7\,\mathrm{T}$). The fit for two measurement configurations ($H_{res\perp}$ and $H_{res\parallel}$) is shown on Fig. 6 by solid lines. The parameters C_{Gd}, Θ and α can be taken from different experiments. The Gd Curie constant C_{Gd} and Curie temperature Θ are known from the susceptibility data of GdOFeAs samples (see Sec. III). As it is shown in Ref. 19 the bulk Fe susceptibility of LaOFeAs samples is determined by the spin susceptibility. Therefore the parameter α can be estimated from this measurement yielding a value of $\sim 10^{-4}$ $\frac{\mathrm{erg}}{\mathrm{G^2\ mol}}$[19,35–37]. The λ value resulting from the fit is equal to ~ 19.7 $\frac{\mathrm{G^2\ mol}}{\mathrm{erg}}$ for $H_{res\perp}$ and ~ 25.3 $\frac{\mathrm{G^2\ mol}}{\mathrm{erg}}$ for $H_{res\parallel}$. According to the mean field theory[32], these values yield an estimate of the exchange interaction energy J for two configurations amounting to $|J| \sim 15\,\mathrm{K}$ for $H_{res\perp}$ and $|J| \sim 19\,\mathrm{K}$ for $H_{res\parallel}$. In addition, Eq. A.1 enables to calculate the uncompensated moment m_{Fe}. Its value grows with decreasing the temperature and increasing the Gd susceptibility until it reaches $\sim 0.03\mu_B$ at the lowest measured temperature.

Since α is very small compared to C_{Gd} and λ, Eq. A.4 can be simplified to the form:

$$H_{int} \sim \pm \frac{\lambda^2 \alpha C_{Gd}}{(T-\Theta)} H_{ext} \tag{A.5}$$

[1] Y. Kamihara, T. Watanabe, M. Hirano, and H. Hosono, J. Am. Chem. Soc. **130**, 32963297 (2008).
[2] X. H. Chen, T. Wu, G. Wu, R. H. Liu, H. Chen, and D. F. Fang, Nature **453**, 761 (2008).
[3] A. J. Drew, C. Niedermayer, P. J. Baker, F. L. Pratt, S. J. Blundell, T. Lancaster, R. H. Liu, G. Wu, X. H. Chen, I. Watanabe, et al., Nat. Mater. **8**, 310 (2009).
[4] C. Hess, A. Kondrat, A. Narduzzo, J. E. Hamann-Borrero, R. Klingeler, J. Werner, G. Behr, and B. Büchner, EPL (Europhysics Letters) **87**, 17005 (2009).
[5] J. Zhao, Q. Huang, C. de la Cruz, S. Li, J. W. Lynn, Y. Chen, M. A. Green, G. F. Chen, G. Li, Z. Li, et al., Nat. Mater. **7**, 953 (2008).
[6] H. Luetkens, H.-H. Klauss, M. Kraken, F. J. Litterst, T. Dellmann, R. Klingeler, C. Hess, R. Khasanov, A. Amato, C. Baines, et al., Nat. Mater. **8**, 305 (2009).
[7] Y. Laplace, J. Bobroff, F. Rullier-Albenque, D. Colson, and A. Forget, Phys. Rev. B **80**, 140501 (2009).
[8] M.-H. Julien, H. Mayaffre, M. Horvatic, C. Berthier, X. D. Zhang, W. Wu, G. F. Chen, N. L. Wang, and J. L. Luo, EPL (Europhysics Letters) **87**, 37001 (5pp) (2009).
[9] S. Sanna, R. De Renzi, T. Shiroka, G. Lamura, G. Prando, P. Carretta, M. Putti, A. Martinelli, M. R. Cimberle, M. Tropeano, et al., Phys. Rev. B **82**, 060508(R) (2010).
[10] R. R. Urbano, E. L. Green, W. G. Moulton, A. P. Reyes, P. L. Kuhns, E. M. Bittar, C. Adriano, T. M. Garitezi, L. Bufaical, and P. G. Pagliuso, Phys. Rev. Lett. **105**, 107001 (2010).
[11] J. P. Carlo, Y. J. Uemura, T. Goko, G. J. MacDougall, J. A. Rodriguez, W. Yu, G. M. Luke, P. Dai, N. Shannon, S. Miyasaka, et al., Phys. Rev. Lett. **102**, 087001 (2009).
[12] C. Bernhard, A. J. Drew, L. Schulz, V. K. Malik, M. Roessle, C. Niedermayer, T. Wolf, G. D. Varma, G. Mu, H. H. Wen, et al., New Journal of Physics **11**, 055050 (2009), 0902.0859.
[13] Y. Nakai, K. Ishida, Y. Kamihara, M. Hirano, and H. Hosono, J. Phys. Soc. Jpn. **77**, 073701 (2008).
[14] G. Prando, P. Carretta, A. Rigamonti, S. Sanna, A. Palenzona, M. Putti, and M. Tropeano, Phys. Rev. B **81**, 100508 (2010).
[15] H. Maeter, H. Luetkens, Y. G. Pashkevich, A. Kwadrin, R. Khasanov, A. Amato, A. A. Gusev, K. V. Lamonova, D. A. Chervinskii, R. Klingeler, et al., Phys. Rev. B **80**, 094524 (2009).
[16] C. Golze, A. Alfonsov, R. Klingeler, B. Büchner, V. Kataev, C. Mennerich, H.-H. Klauss, M. Goiran, J.-M. Broto, H. Rakoto, et al., Phys. Rev. B **73**, 224403 (2006).
[17] A. Kondrat, J. E. Hamann-Borrero, N. Leps, M. Kosmala, O. Schumann, A. Köhler, J. Werner, G. Behr, M. Braden, R. Klingeler, et al., Eur. Phys. J. B **70 (4)**, 461-468 (2009).
[18] N. D. Zhigadlo, S. Katrych, Z. Bukowski, S. Weyeneth, R. Puzniak, and J. Karpinski, Journal of Physics: Condensed Matter **20**, 342202 (2008).
[19] R. Klingeler, N. Leps, I. Hellmann, A. Popa, U. Stockert, C. Hess, V. Kataev, H. Grafe, F. Hammerath, G. Lang, et al., Phys. Rev. B **81**, 024506 (2010).
[20] H.-H. Klauss, H. Luetkens, R. Klingeler, C. Hess, F. J. Litterst, M. Kraken, M. M. Korshunov, I. Eremin, S.-L. Drechsler, R. Khasanov, et al., Phys. Rev. Lett. **101**, 077005 (2008).
[21] N. D. Zhigadlo, S. Katrych, S. Weyeneth, R. Puzniak, P. J. W. Moll, Z. Bukowski, J. Karpinski, H. Keller, and B. Batlogg, Phys. Rev. B **82**, 064517 (2010).
[22] M. Rotter, M. Pangerl, M. Tegel, and D. Johrendt, Angew. Chem. **47**, 7949 (2008), 0807.4096.
[23] A. Koitzsch, D. S. Inosov, D. V. Evtushinsky, V. B. Zabolotnyy, A. A. Kordyuk, A. Kondrat, C. Hess, M. Knupfer, B. Büchner, G. L. Sun, et al., Phys. Rev. Lett. **102**, 167001 (2009).
[24] A. Kondrat, G. Behr, B. Büchner, and C. Hess (2010), 1006.0715.
[25] S. E. Barnes, Adv. Phys. **30**, 801 (1981).
[26] A. Abragam and B. Bleaney, *Electron Paramagnetic Resonance of Transition Ions* (1970).
[27] E. Dengler, J. Deisenhofer, H.-A. Krug von Nidda, S. Khim, J. S. Kim, K. H. Kim, F. Casper, C. Felser, and A. Loidl, Phys. Rev. B **81**, 024406 (2010).
[28] G. F. Goya, R. C. Mercader, L. B. Stere, R. D. Sánchez, M. T. Causa, and M. Tovar, J. Phys.: Condens. Matter **8**, 4529 (1996).
[29] C. de la Cruz, Q. Huang, J. W. Lynn, J. Li, W. Ratcliff II, J. L. Zarestky, H. A. Mook, G. F. Chen, J. L. Luo, N. L. Wang, et al., Nature **453**, 899 (2008).
[30] A. Fainstein, A. Butera, and M. Tovar, Phys. Rev. B **50**, 16708 (1994).
[31] S. B. Oseroff, D. Rao, F. Wright, D. C. Vier, S. Schultz, J. D. Thompson, Z. Fisk, S.-W. Cheong, M. F. Hundley, and M. Tovar, Phys. Rev. B **41**, 1934 (1990).
[32] C. Kittel, *Introduction to Solid State Physics* (WILEY, 2005).

[33] S. Shamoto, M. Ishikado, S. Wakimoto, K. Kodama, R. Kajimoto, M. Arai, T. Fukuda, H. Nakamura, M. Machida, and H. Eisaki, Physica C: Superconductivity **470**, S284 (2009).
[34] S. Wakimoto, K. Kodama, M. Ishikado, M. Matsuda, R. Kajimoto, M. Arai, K. Kakurai, F. Esaka, A. Iyo, H. Kito, et al., J. Phys. Soc. Jpn. **79**, 074715 (2010).
[35] M. A. McGuire, A. D. Christianson, A. S. Sefat, B. C. Sales, M. D. Lumsden, R. Jin, E. A. Payzant, D. Mandrus, Y. Luan, V. Keppens, et al., Phys. Rev. B **78**, 094517 (2008).
[36] T. Nomura, S. W. Kim, Y. Kamihara, M. Hirano, P. V. Sushko, K. Kato, M. Takata, A. L. Shluger, and H. Hosono, Supercond. Sci. Technol. **21**, 125028 (2008), 0804.3569.
[37] Y. Kohama, Y. Kamihara, M. Hirano, H. Kawaji, T. Atake, and H. Hosono, Phys. Rev. B **78**, 020512 (2008).
[38] Note here that a dysonian ESR line shape, which is typical for metallic samples in a cavity, is not observed here due to the fine grinding of the sample and further mixing with epoxy. This procedure reduces the microwave dispersion which is the origin of the dysonian line shape.
[39] For simplicity which does not affect the conclusions of the following qualitative discussion, we assume hereafter that the uncompensated magnetic moments and thereby created internal fields are collinear with the applied magnetic field.